Selection of element-wise shell kinematics using neural networks

# Selection of element-wise shell kinematics using neural networks

M. Petrolo[*], E. Carrera[†]

MUL$^2$ Group, Department of Mechanical and Aerospace Engineering, Politecnico di Torino
Turin, Italy

Submitted to
Computers and Structures

*Author for correspondence:*
Marco Petrolo
MUL$^2$ Group, Department of Mechanical and Aerospace Engineering,
Politecnico di Torino,
Corso Duca degli Abruzzi 24,
10129 Torino, Italy,
tel: +39 011 090 6845,
fax: +39 011 090 6899,
e-mail: erasmo.carrera@polito.it

[*]Associate Professor, marco.petrolo@polito.it
[†]Professor of Aerospace Structures and Aeroelasticity, erasmo.carrera@polito.it

## *Abstract*

*This paper presents a novel approach to evaluate the role of non-classical effects, e.g., shear deformability, over a shell finite element model. Such an approach can identify the areas of a structural model in which the use of first-order shear deformation theories may lead to significant inaccuracies. Furthermore, it can indicate optimal distributions of structural theories over the finite element mesh to trade-off accuracy and computational costs. The proposed framework exploits the synergies among four methods, namely, the Carrera Unified Formulation (CUF), the Finite Element Method (FEM), the Node-Dependent Kinematics (NDK), and Neural Networks (NN). CUF generates the FE matrices for higher-order shell theories and provides numerical results feeding the NN for training. Via NDK, the shell theory is a property of the node; that is, a distribution of various shell theories over the FE mesh is attainable. The distributions of theories and the thickness of the structure are the inputs of multilayer NN to target natural frequencies. This work investigates the accuracy and cost-effectiveness of well-known NN. The results look promising as the NN requires a fraction of FE analyses for training, can evaluate the accuracy of FE models, and can incorporate physical features, e.g., the thickness ratio, that drives the complexity of the mathematical model. In other words, NN can inform on the FE modeling without the need to modify, rebuild, or rerun an FE model.*

# 1 Introduction

The accuracy of shell finite elements (FE) depends on the problem in hand, and the kinematics adopted over the thickness. Usually, the kinematics is the same for every node and element of the model. For instance, shell elements have kinematics from the classical theories of structures, namely, the classical lamination theory (CLT) and the first-order shear deformation theory (FSDT) [1–6], with a maximum number of six nodal degrees of freedom (DOF), namely, three displacements and rotations. Recently, the node dependent kinematics (NDK) [7, 8] has allowed one to build FE models in which the kinematics is a property of the node; that is, each node can have different structural theories with the aim to use refined models only where necessary.

Refined kinematics is necessary to overcome the limitations of classical models whose accuracy is high if the structure is thin, there are no local effects, and in-plane stress and transverse displacements are of interest. The limitations of classical models are particularly relevant in the case of composite structures. Several phenomena fall beyond the prediction capabilities of classical models [9, 10]; e.g., high transverse deformability and anisotropy, edge-effects, local distortions, higher-order oscillations, cracks, contacts, and multifield interactions in which the material characteristics can change significantly and anisotropically. Over the years, many refinement strategies have emerged to include shear and normal transverse stresses, and variations of the displacement field at the interface between two layers with different mechanical properties, i.e., the zig-zag effect [11–22].

The present paper considers the free vibration analysis of composite shells via FEM. Many efforts focused on the development of exact, analytical, or semi-analytical solutions to verify numerical approaches. Leissa and Reddy are among the main contributors with special attention paid to 3D solutions and shear deformation theories [16, 23, 24]. Comprehensive reviews on this topic are available in Qatu's works [25, 26]. A brief overview of works focused on the free vibration analysis via shell FE follows.

The finite element method (FEM) emerged a few decades ago [27–29]. The research activity focused on the element type, i.e., four- [30–32], eight- [33, 34], and nine-node elements [35, 36]. and the the order of the structural model [37–40]. Recent works aimed to improve numerical solutions via various approaches, e.g., assumed strain FE [41], wave FE and wave based method [42, 43], Haar wavelet method [44, 45], spline collocation and convolution method [46–48], and the reverberation ray matrix [49].

This paper proposes the use of neural networks (NN) to select the shell kinematics at the FE level

and identify the regions of a structure in which the refined kinematics has a primary importance. The underlying idea behind NN stems from biological nervous systems and leads to simple computational units interlinked by a system of connections [50] with the aim of learning through training and samples. The use of NN in structural and material simulation is increasing due to the superior computational efficiency [51–53]. Recent applications for composites and FE concern the prediction of the elastic properties [54, 55], buckling load [56], strength and failure analyses [57–61], structural dynamics [62–65], virtual manufacturing [66, 67], linear and nonlinear analyses [68–70], and optimization [71, 72].

This paper combines NN with the Carrera unified formulation (CUF), the axiomatic/asymptotic method (AAM), and the node dependent kinematics (NDK). CUF [73] provides the governing equations for all the structural models, independently of the order of the theory or the completeness of the expansions. Similarly, the FE version of CUF [74] obtains all the FE matrices and arrays compactly and independently of the order of the structural theory. AAM [75, 76] is a method to evaluate the accuracy of any structural theory. Two of the outcomes provided by the AAM are the best theory diagram (BTD) [77] and the relevance factor (RF) [78]. BTD is a 2D plot to localize a structural theory via its nodal degrees of freedom and accuracy. RF is a parameter providing the relevance of a generalized variable or a set of variables.

Refined structural theories can tackle several mechanical phenomena. Given a structural problem, the spatial distribution of such phenomena can vary significantly. For instance, the proximity of geometrical and mechanical boundary conditions can require the use of refined models. The necessity to use refined models in an area of the structure signals the presence of non-classical effects. NDK offers the capability of locally inserting refined models by allowing a node-wise distribution of structural theories [7, 8]. This paper presents a novel strategy to evaluate the best distributions of shell theories over a 2D mesh, and, therefore, to determine the most critical areas to model.

This paper is organized as follows: the governing equations and the methodology are in Sections 2, 3, and 4; results in Section 5, and conclusions in Section 6.

## 2 CUF and finite element formulation

Using the reference frame in Fig. 1, the CUF displacement field for a 2D model is

$$\mathbf{u}(x,y,z) = F_\tau(z)\mathbf{u}_\tau(x,y) \qquad \tau = 1,\ldots,M \tag{1}$$

The Einstein notation acts on $\tau$. $\mathrm{F}_\tau$ are the thickness expansion functions. $\mathbf{u}_\tau$ is the vector of the generalized unknown displacements. M is the number of expansion terms. In the case of polynomial,

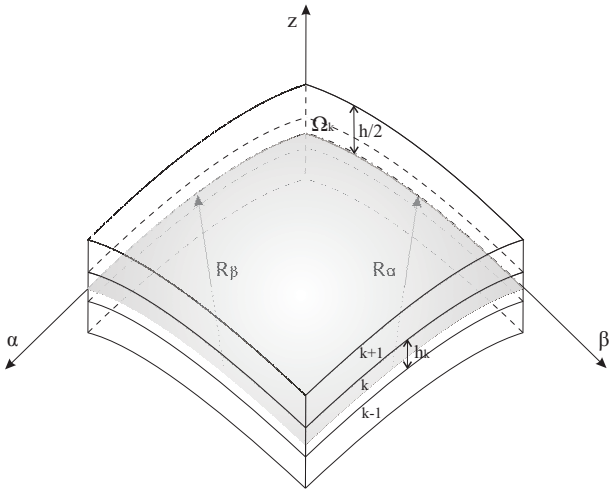


Figure 1: Shell geometry

Taylor-like expansions, a fourth-order model, referred to as N=4, has the following displacement field:

$$\begin{aligned} u_\alpha &= u_{\alpha_1} + z\,u_{\alpha_2} + z^2\,u_{\alpha_3} + z^3\,u_{\alpha_4} + z^4\,u_{\alpha_5} \\ u_\beta &= u_{\beta_1} + z\,u_{\beta_2} + z^2\,u_{\beta_3} + z^3\,u_{\beta_4} + z^4\,u_{\beta_5} \\ u_z &= u_{z_1} + z\,u_{z_2} + z^2\,u_{z_3} + z^3\,u_{z_4} + z^4\,u_{z_5} \end{aligned} \tag{2}$$

N=4 has fifteen nodal DOF. The order and type of expansion is a free parameter. Thus, the structure of the theory is an input of the analysis. The metric coefficients $\mathrm{H}^k_\alpha$, $\mathrm{H}^k_\beta$ and $\mathrm{H}^k_z$ of the $\mathrm{k}^{th}$ layer are

$$H^k_\alpha = A^k(1 + z_k/R^k_\alpha), \quad H^k_\beta = B^k(1 + z_k/R^k_\beta), \quad H^k_z = 1 \tag{3}$$

$\mathrm{R}^k_\alpha$ and $\mathrm{R}^k_\beta$ are the principal radii of the middle surface of the $\mathrm{k}^{th}$ layer, $\mathrm{A}^k$ and $\mathrm{B}^k$ the coefficients of the first fundamental form of $\Omega_k$, see Fig. 1. This paper focuses only on shells with constant radii of

curvature with $\mathrm{A}^k = \mathrm{B}^k = 1$. The geometrical relations are

$$\begin{aligned} \boldsymbol{\epsilon}_p^k &= \left\{ \epsilon_{\alpha\alpha}^k, \epsilon_{\beta\beta}^k, \epsilon_{\alpha\beta}^k \right\}^T = (\boldsymbol{D}_p^k + \boldsymbol{A}_p^k)\boldsymbol{u}^k \\ \boldsymbol{\epsilon}_n^k &= \left\{ \epsilon_{\alpha z}^k, \epsilon_{\beta z}^k, \epsilon_{zz}^k \right\}^T = (\boldsymbol{D}_{n\Omega}^k + \boldsymbol{D}_{nz}^k - \boldsymbol{A}_n^k)\boldsymbol{u}^k \end{aligned} \tag{4}$$

where

$$\boldsymbol{D}_p^k = \begin{bmatrix} \frac{\partial_\alpha}{H_\alpha^k} & 0 & 0 \\ 0 & \frac{\partial_\beta}{H_\beta^k} & 0 \\ \frac{\partial_\beta}{H_\beta^k} & \frac{\partial_\alpha}{H_\alpha^k} & 0 \end{bmatrix} \quad \boldsymbol{D}_{n\Omega}^k = \begin{bmatrix} 0 & 0 & \frac{\partial_\alpha}{H_\alpha^k} \\ 0 & 0 & \frac{\partial_\beta}{H_\beta^k} \\ 0 & 0 & 0 \end{bmatrix} \quad \boldsymbol{D}_{nz}^k = \begin{bmatrix} \partial_z & 0 & 0 \\ 0 & \partial_z & 0 \\ 0 & 0 & \partial_z \end{bmatrix} \tag{5}$$

$$\boldsymbol{A}_p^k = \begin{bmatrix} 0 & 0 & \frac{1}{H_\alpha^k R_\alpha^k} \\ 0 & 0 & \frac{1}{H_\beta^k R_\beta^k} \\ 0 & 0 & 0 \end{bmatrix} \quad \boldsymbol{A}_n^k = \begin{bmatrix} \frac{1}{H_\alpha^k R_\alpha^k} & 0 & 0 \\ 0 & \frac{1}{H_\beta^k R_\beta^k} & 0 \\ 0 & 0 & 0 \end{bmatrix} \tag{6}$$

The stress-strain relations are

$$\begin{aligned} \boldsymbol{\sigma}_p^k &= \left\{ \sigma_{\alpha\alpha}^k, \sigma_{\beta\beta}^k, \sigma_{\alpha\beta}^k \right\}^T = \boldsymbol{C}_{pp}^k \boldsymbol{\epsilon}_p^k + \boldsymbol{C}_{pn}^k \boldsymbol{\epsilon}_n^k \\ \boldsymbol{\sigma}_n^k &= \left\{ \sigma_{\alpha z}^k, \sigma_{\beta z}^k, \sigma_{zz}^k \right\}^T = \boldsymbol{C}_{np}^k \boldsymbol{\epsilon}_p^k + \boldsymbol{C}_{nn}^k \boldsymbol{\epsilon}_n^k \end{aligned} \tag{7}$$

where

$$\begin{aligned} \boldsymbol{C}_{pp}^k &= \begin{bmatrix} C_{11}^k & C_{12}^k & C_{16}^k \\ C_{12}^k & C_{22}^k & C_{26}^k \\ C_{16}^k & C_{26}^k & C_{66}^k \end{bmatrix} \quad \boldsymbol{C}_{pn}^k = \begin{bmatrix} 0 & 0 & C_{13}^k \\ 0 & 0 & C_{23}^k \\ 0 & 0 & C_{36}^k \end{bmatrix} \\ \boldsymbol{C}_{np}^k &= \begin{bmatrix} 0 & 0 & 0 \\ 0 & 0 & 0 \\ C_{13}^k & C_{23}^k & C_{36}^k \end{bmatrix} \quad \boldsymbol{C}_{nn}^k = \begin{bmatrix} C_{55}^k & C_{45}^k & 0 \\ C_{45}^k & C_{44}^k & 0 \\ 0 & 0 & C_{33}^k \end{bmatrix} \end{aligned} \tag{8}$$

The FEM formulation adopts a nine-node shell element based on the Mixed Interpolation of Tensorial Component (MITC) method [79]. The displacement vector becomes

$$\delta \boldsymbol{u}_s = N_j \delta \boldsymbol{u}_{sj}, \qquad \boldsymbol{u}_\tau = N_i \boldsymbol{u}_{\tau i} \qquad i, j = 1, \cdots, 9 \tag{9}$$

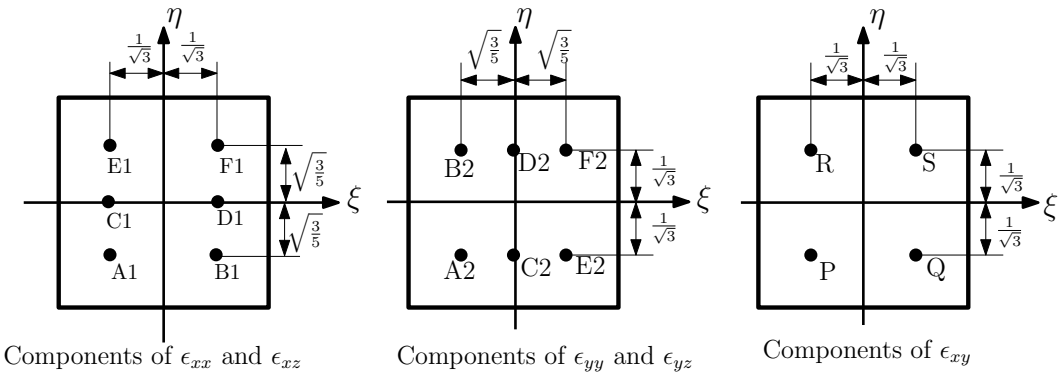


Figure 2: MITC9 tying points

$\boldsymbol{u}_{\tau i}$ and $\delta\boldsymbol{u}_{sj}$ are the nodal displacement vector and the virtual displacement, respectively. The strain expression becomes

$$\begin{aligned}\boldsymbol{\epsilon}_p &= F_\tau(\boldsymbol{D}_p + \boldsymbol{A}_p)N_i\boldsymbol{u}_{\tau i}\\ \boldsymbol{\epsilon}_n &= F_\tau(\boldsymbol{D}_{n\Omega} - \boldsymbol{A}_n)N_i\boldsymbol{u}_{\tau i} + F_{\tau,z}N_i\boldsymbol{u}_{\tau i}\end{aligned} \tag{10}$$

MITC avoids the membrane and shear locking via a specific interpolation strategy for the strain components on the nine-node shell element, as follows:

$$\begin{aligned}\boldsymbol{\epsilon}_p &= \begin{bmatrix}\epsilon_{\alpha\alpha}\\ \epsilon_{\beta\beta}\\ \epsilon_{\alpha\beta}\end{bmatrix} = \begin{bmatrix}N_{m1} & 0 & 0\\ 0 & N_{m2} & 0\\ 0 & 0 & N_{m3}\end{bmatrix}\begin{bmatrix}\epsilon_{\alpha\alpha_{m1}}\\ \epsilon_{\beta\beta_{m2}}\\ \epsilon_{\alpha\beta_{m3}}\end{bmatrix}\\ \boldsymbol{\epsilon}_n &= \begin{bmatrix}\epsilon_{\alpha z}\\ \epsilon_{\beta z}\\ \epsilon_{zz}\end{bmatrix} = \begin{bmatrix}N_{m1} & 0 & 0\\ 0 & N_{m2} & 0\\ 0 & 0 & 1\end{bmatrix}\begin{bmatrix}\epsilon_{\alpha z_{m1}}\\ \epsilon_{\beta z_{m2}}\\ \epsilon_{z z_{m3}}\end{bmatrix}\end{aligned} \tag{11}$$

Strains $\epsilon_{\alpha\alpha_{m1}}$, $\epsilon_{\beta\beta_{m2}}$, $\epsilon_{\alpha\beta_{m3}}$, $\epsilon_{\alpha z_{m1}}$, and $\epsilon_{\beta z_{m2}}$ result from Eq. 10 and

$$\begin{aligned}N_{m1} &= [N_{A1}, N_{B1}, N_{C1}, N_{D1}, N_{E1}, N_{F1}]\\ N_{m2} &= [N_{A2}, N_{B2}, N_{C2}, N_{D2}, N_{E2}, N_{F2}]\\ N_{m3} &= [N_P, N_Q, N_R, N_S]\end{aligned} \tag{12}$$

Subscripts m1, m2 and m3 indicate the point groups (A1,B1,C1,D1,E1,F1), (A2,B2,C2,D2,E2,F2), and (P,Q,R,S), respectively, see Fig. 2.

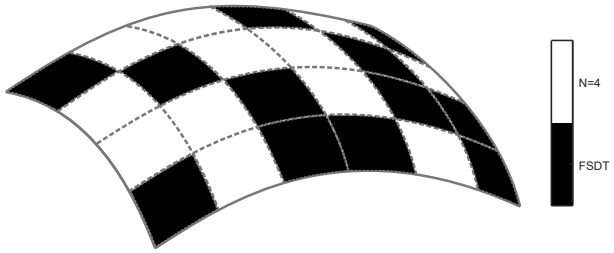


Figure 3: Distribution of FSDT and fourth-order shell theories over a 2D mesh

According to the Principle of Virtual Displacements (PVD),

$$\int_{\Omega_k}\int_{A_k} \delta\boldsymbol{\epsilon}^{k^T}\boldsymbol{\sigma}^k H^k_\alpha H^k_\beta d\Omega_k dz + \int_{\Omega_k}\int_{A_k} \rho^k \delta\boldsymbol{u}^{k^T}\ddot{\boldsymbol{u}}^k H^k_\alpha H^k_\beta d\Omega_k dz = 0 \tag{13}$$

$\Omega_k$ is the in-plane domain of a layer over the element, and $A_k$ is the thickness one. Via the constitutive equations, geometrical, MITC and CUF relations, the following governing equation reads

$$\boldsymbol{m}^k_{\tau isj}\ddot{\boldsymbol{u}}^k_{\tau i} + \boldsymbol{k}^k_{\tau sij}\boldsymbol{u}^k_{\tau i} = 0 \tag{14}$$

$\boldsymbol{k}^k_{\tau sij}$ and $\boldsymbol{m}^k_{\tau sij}$ are 3×3 matrices referred to as the fundamental nucleus of the stiffness and mass matrices, respectively. The components of the nuclei are given in [74]. The assembly over all nodes and elements and the introduction of the harmonic solution leads to the well-known eigenvalue problem,

$$(-\omega_n^2\boldsymbol{M} + \boldsymbol{K})\boldsymbol{U}_n = 0 \tag{15}$$

In CUF, the shell theory is a property of the node. In other words, each node can have a shell theory, and the neighbor nodes others. In this work, the shell theory is the same for each node of an element; FSDT and N=4 are the models adopted. Figure 3 shows an example of a shell mesh in which each element is either N=4 or FSDT. For more details on NDK, the reader may refer to [7, 8].

## 3 Axiomatic/asymptotic method and best theory distributions

The axiomatic/asymptotic method (AAM) is a methodology to assess the influence of generalized variables and the accuracy of structural models [75, 76]. In previous works, AAM acted on the set of variables of the expansion, e.g., in the case of N=4, AAM considered the fifteen primary variables and evaluated

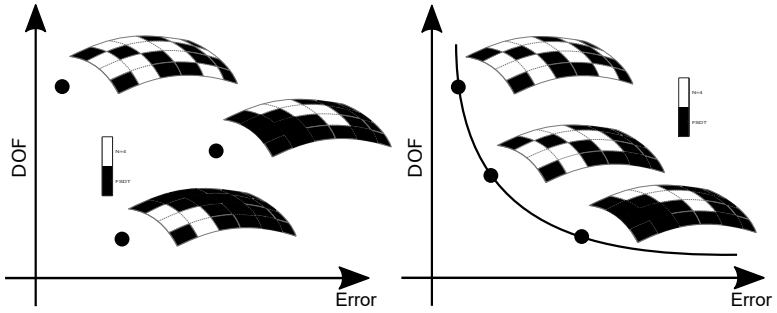


(a) Three shell theory distributions (b) Best Theory Distributions (BTD)

Figure 4: FE distributions in a 2D Cartesian reference frame and an example of BTD

their influence. In the present paper, AAM acts on the distribution of shell theories over a given mesh. For instance, in the case of a 4×4 mesh, AAM evaluates the accuracy of every combination of FSDT and N=4, as shown in Fig. 3. Overall, $2^{16}$ mesh distributions are evaluated. The implementation of the AAM may follow various approaches; in this work:

1. Definition of parameters such as geometry, boundary conditions, materials, and layer layouts.

2. Axiomatic choice of a starting theory and definition of the starting nodal unknowns. Usually, the starting theory provides 3D-like solutions. The fourth-order, equivalent single-layer shell model is the reference model of this paper.

3. Definition of a FEM mesh. In this work, a 4×4 mesh nine-node mesh was used as, for the considered problems provides good accuracy.

4. The CUF generates the governing equations for the theory distributions considered.

5. For each structural theory distribution, the accuracy evaluation makes use of one or more control parameters; in this paper, the first ten natural frequencies.

6. The analysis is carried out multiple times to evaluate the relevance of problem parameters, e.g., thickness, orthotropic ratio, stacking sequence, boundary conditions.

Two parameters can identify a distribution, namely, the number of DOF of the model and the error or accuracy provided. The use of two parameters allows the insertion of each FE distribution in a Cartesian reference frame, as in Fig. 4a. The Best Theory Distribution (BTD) is the curve composed of all meshes with a given number of N=4 and FSDT elements providing the minimum error, see Fig. 4b. In the case

of sixteen elements, the BTD will have sixteen models, the first one with all N=4 and the last one with all FSDT. To have a single error parameter, the BTD uses the average of the errors as follows:

$$Error = \sum_{i=1}^{10} \frac{f_i / f_i^{N=4}}{10} \tag{16}$$

Where $f_i$ is the i-th frequency from a generic shell model, and $f_i^{N=4}$ is the one from the reference solution and having fourt-order kinematics in all elements.

## 4 Neural networks and coding

CUF FE analyses generate inputs to train NN. In this paper, the inputs are the structural theories of the elements and the thickness ratio, and outputs are the errors over the first ten frequencies. Figure 5 shows the two ways adopted in this paper to build the BTD, i.e.,

- CUF generates the governing FE equations for all the shell FE models from combinations of FSDT and N=4 distributions. Given a 4×4 mesh, overall, $2^{16}$ FE shell models are available. The two limit cases are those in which all elements are FSDT, or all are N=4.
- The FE way runs $2^{16}$ analyses and reports the error and number of FSDT and N=4 elements in a 2D plot.
- The NN way runs one-tenth of the FE analyses and uses them for training. Then, the 2D plot stems from querying the trained NN with all $2^{16}$ shell models.
- If a/h is a training variable, and, e.g., three a/h values are available, the overall number of analyses is $3 \times 2^{16}$, and the query of the NN includes the thickness ratio.

The aim is to build the BTD with less than $2^{16}$ analyses and avoid new FE analyses as the thickness ratio changes. In Fig. 5, the NN training set has 10% of all analyses, as this is a typical value used in this paper. Also, the figure shows only one hidden layer, although more layers could be necessary.

The NN is a multilayer feed-forward with early stopping and the mean squared error as the objective function. Depending on the numerical case, each layer has ten to twenty neurons, and three to six layers are used. This paper adopts Levenberg-Marquardt training functions [80]. The input coding is a vector with seventeen elements, that is, all the elements of the FE model and the thickness ratio. Each element

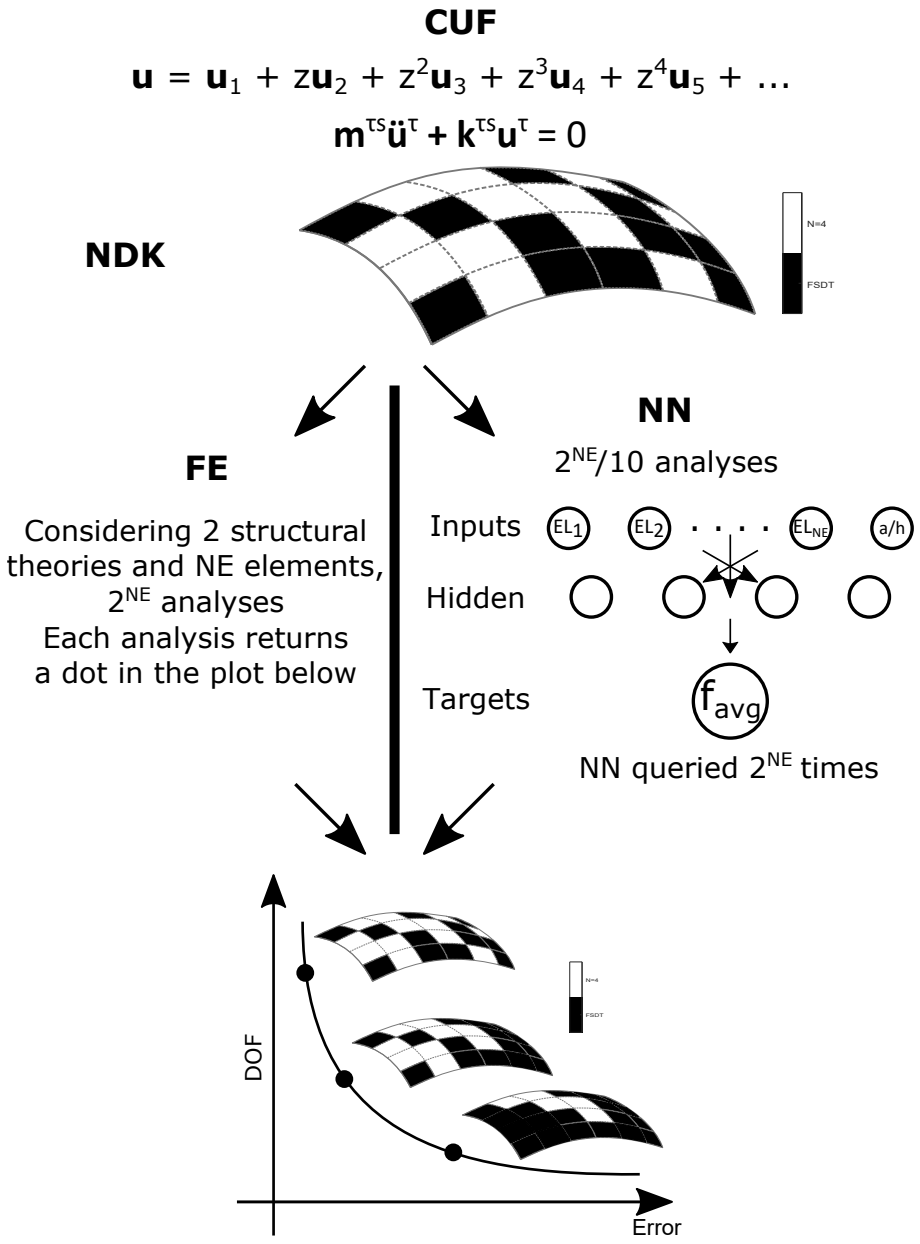


Figure 5: CUF, NDK and NN framework

Table 1: S-S, 0/90/0, a/h=10, $\overline{\omega}=\omega\sqrt{\frac{\rho a^4}{h^2 E_T}}$

| Model | |
|---|---|
| HSDT [24] | 12.060 |
| FSDT [23] | 12.372 |
| CLT [84] | 15.233 |
| LD4 [81] | 11.685 |
| N=4 | 11.972 |

status is either '1' or '0' to indicate an N=4 or FSDT structural theory, respectively. Each input has an associated output composed of a vector containing the error, Eq. 16.

# 5 Results

The numerical results consider spherical shells with geometrical and material characteristics retrieved from [24, 78, 81, 82]. The shell has a=b, $R_\alpha$=$R_\beta$=R, and R/a=5. The material properties are $E_1/E_2$=25, $G_{12}/E_2$=$G_{13}/E_2$=0.5, $G_{13}/E_2$=0.2, $\nu$=0.25. The accuracy of the FE models is computed over the first ten frequencies of symmetric modal shapes, and the FE considers a quarter of shell via a 4×4 mesh as in [78]. The analysis of symmetric modes allowed us to use a reduced number of elements via symmetric boundary conditions with a significantly lower computational cost. As shown in [83], the constraint on the symmetric modes does not modify the results to a great extent.

## 5.1 Evaluation of NN with fixed thickness ratio

The first assessment deals with a moderately-thick shell and two sets of boundary conditions and stacking sequences. The first set is simply-supported (S-S) on all edges; the second one has the top and bottom edges clamped and the lateral ones free (C-F). This set of analyses aims to evaluate the accuracy of the NN for a given thickness ratio before adding a/h as a training feature.

Table 1 shows the first natural frequency from different models, including higher- and first-order shear deformation theories, HSDT and FSDT, respectively, classical lamination theory, CLT, a layer-wise fourth-order model, LD4, and the present equivalent single layer full fourth-order expansion, N=4. The latter, obtained via a 4×4 mesh, provides good accuracy if compared to LD4 and is set as the reference solution to build the BTD. Figure 6 shows the error given by each of the $2^{16}$ mesh combinations. For the sake of readability, some 20% of all cases are shown and randomly picked. The results from the complete

FE solution, and the ones from NN are reported. As mentioned above, the NN solution uses 10% of $2^{16}$ FE analyses for its training and, then, obtains all cases. The vertical axis reports the ratio between the total DOF of a given mesh and the total DOF in the case of the mesh with only fourth-order shell theories. The boundary values are D=1, i.e., fifteen DOF per node and 1215 in total, and D=0.333, i.e., five DOF per node and 405 overall. Figure 7 shows the mesh configurations with the minimum error. The vertical axis reports the number of elements with the fourth-order shell theory and ranging from sixteen - all N=4 - to zero - all FSDT. As in the previous plot, the FE and NN solutions are reported. Figure 8 shows some of the mesh configurations from the previous plot. Mesh distributions having four, eight, and twelve elements with fourth-order kinematics are shown with the error, E, indicated in the captions. Such figures show where the higher-order kinematics is relevant. E.g., considering four N=4 elements, the best configurations shown indicate the zones in which those elements are more necessary to minimize the error. The same plots for the 90/0 lamination are given in Figs. 9, 10 and 11. The results suggest the following:

- The maximum error - given by the use of all FSDT elements - is about 12% for 0/90/0 and 10% for 0/90, and there is a quite linear behavior of the BTD as the number of N=4 elements changes. In all cases, the use of N=4 elements over 75% of the mesh ensures errors smaller than 1-2%.

- The zones of the mesh in which the refined shell kinematics is necessary are highly influences by the geometrical boundary conditions and, to a smaller extent, by the stacking sequence. In the S-S case, the areas with higher deformations, i.e., those far from the supports, require the refined kinematics first. In the C-F case, the clamped zones are those more critical.

- The NN can obtain the FE results with high accuracy and a perfect match if the BTD is considered. This result is relevant by considering that the NN required only 10% of FE analyses and, given that both training and use of NN needed a fraction of the computational costs of FE - In a laptop with four cores, the total time required by training and use of NN is smaller than five minutes- it can be stated that NN can obtain the FE results with one-tenth of the computational time.

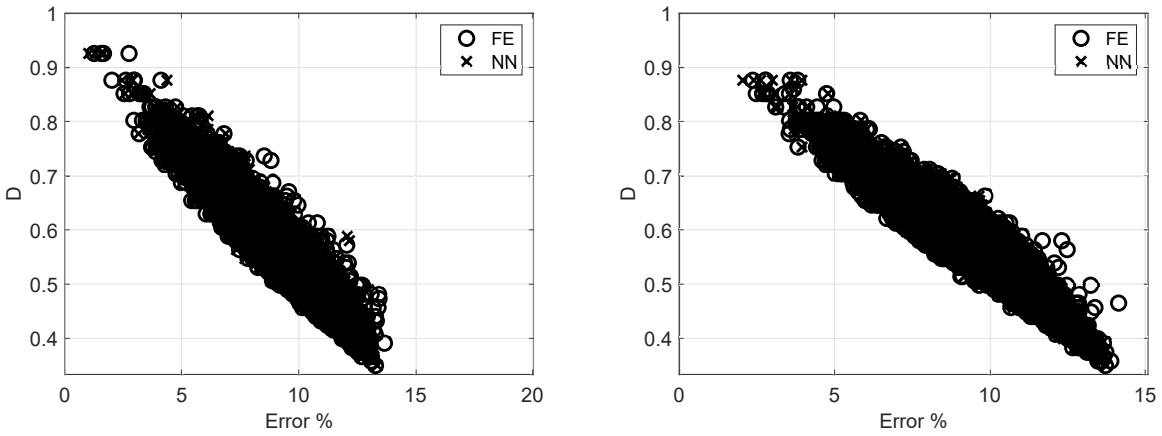


(a) S-S (b) C-F

Figure 6: All combinations for 0/90/0, a/h=10

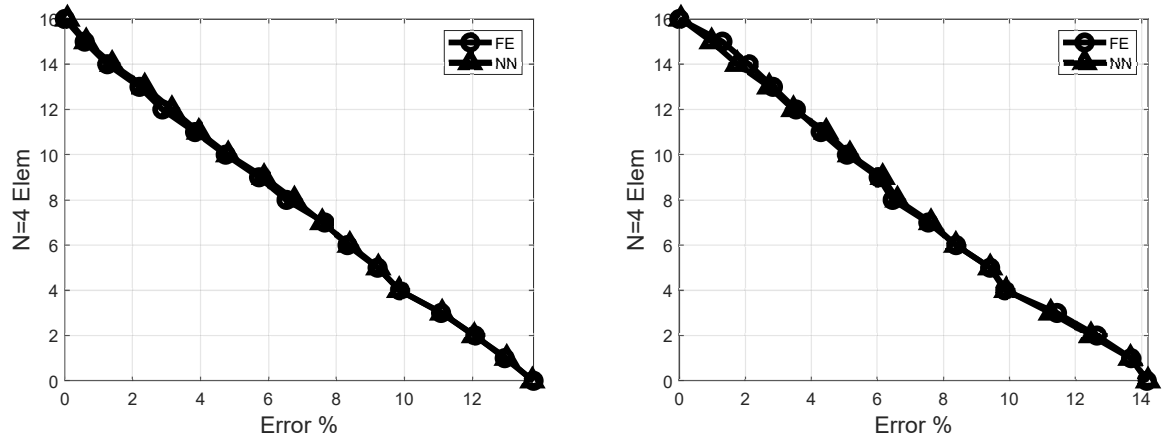


(a) S-S (b) C-F

Figure 7: BTD for 0/90/0, a/h=10

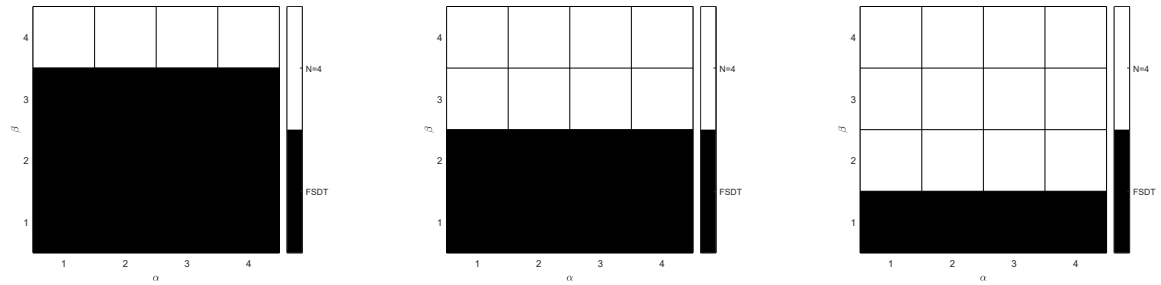


(a) S-S, a/h=10, twelve FSDT, E=9.9 % (b) S-S, a/h=10, eight FSDT, E=6.8 % (c) S-S, a/h=10, four FSDT, E=3.2 %

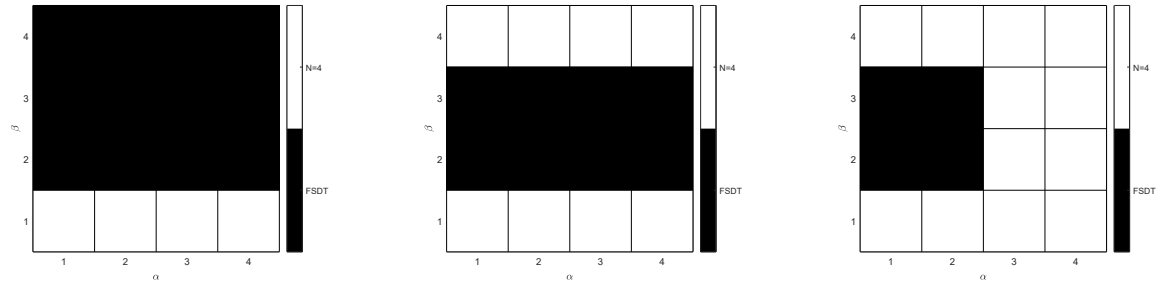


(d) C-F, a/h=10, twelve FSDT, E=9.9 % (e) C-F, a/h=10, eight FSDT, E=6.6 % (f) C-F, a/h=10, four FSDT, E=3.5 %

Figure 8: Best mesh distributions for 0/90/0

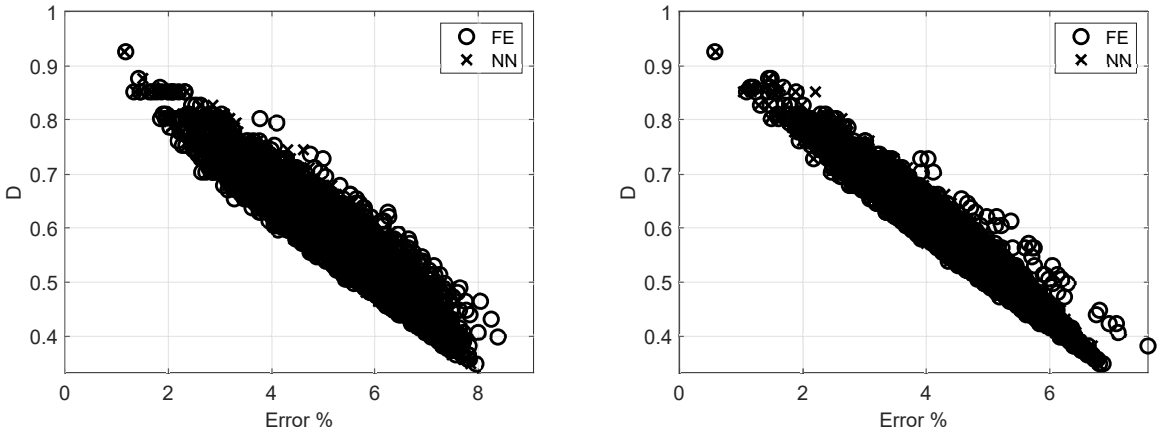


(a) S-S (b) C-F

Figure 9: All combinations for 90/0, a/h=10

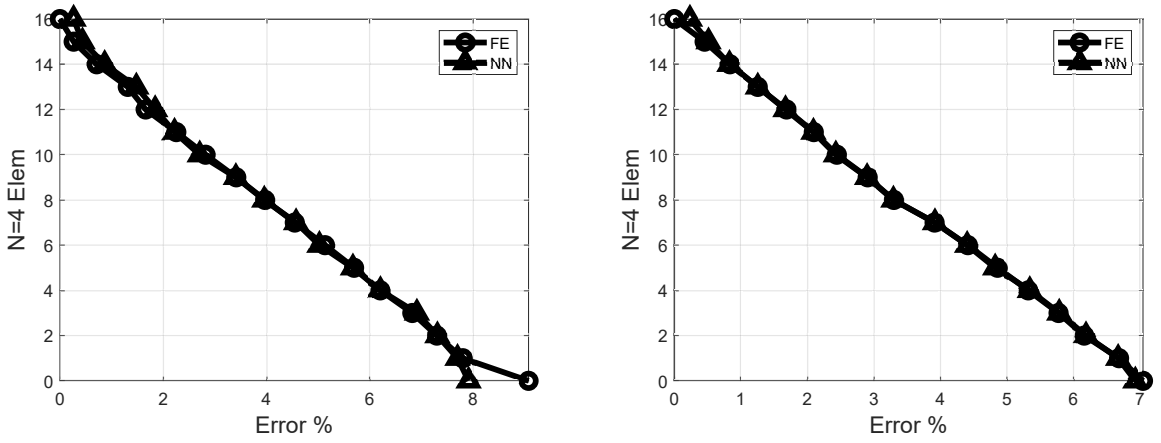


(a) S-S (b) C-F

Figure 10: BTD for 90/0, a/h=10

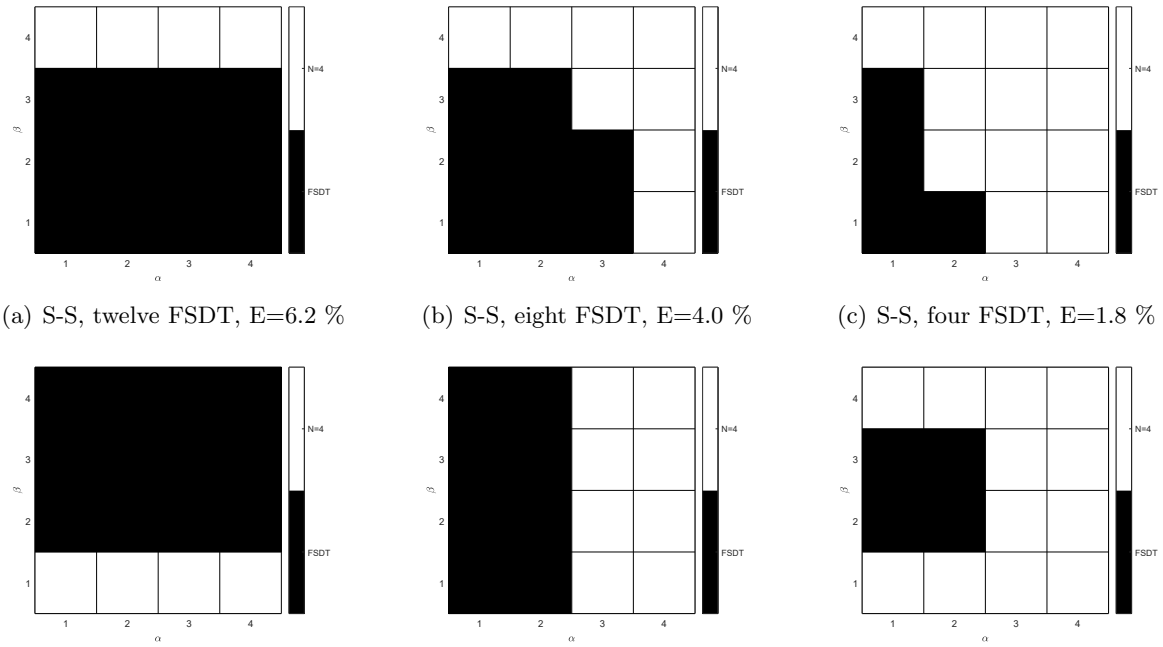


(a) S-S, twelve FSDT, E=6.2 % (b) S-S, eight FSDT, E=4.0 % (c) S-S, four FSDT, E=1.8 %

(d) C-F, twelve FSDT, E=5.3 % (e) C-F, eight FSDT, E=3.3 % (f) C-F, four FSDT, E=1.7 %

Figure 11: Best mesh distributions for 90/0, a/h=10

### 5.2 Evaluation of NN with a/h as a training feature

The second set of results concerns the use of a/h as an additional training feature. For instance, two thickness ratios are used for the FE analyses and to train the NN; then, the NN is used to obtain the results for a third thickness ratio with no need for new FE analyses. The S-S, 0/90/0 shell of the previous section, is used.

Figure 12 shows the BTD for three thickness ratios, namely, 75, 50 and 25. FE and NN results are compared, and, as indicated in the sub-captions, the NN training used two ratios. The aim is to investigate the accuracy of NN in detecting the results within the range of the training. Figure 13 shows the best mesh distributions with four, eight, and twelve FSDT or N=4 theories, together with the error. The results obtained by FE and NN are compared. Similarly, Figs. 14 and 15 shows the results for the other two a/h values. The results suggest that

- Considering the BTD, the accuracy of NN is good. Some discrepancies are visible in the lower part of the plot for a/h=50 and 25. Most likely, the differences are due to the FSDT at a/h=25, 75, 50, and a/h=10, i.e., a/h of the training sets. For a/h=75 such difference is not present as for a/h=50 and 100, FSDT provides similar accuracy.

- The mesh distributions with the best accuracy are very well predicted by NN. There are a few differences for a/h=50, four FSDT, and a/h=75, eight FSDT. In both cases, the difference is due to only one element.

- Considering the results of the previous section for a/h=10, three best mesh distributions were found. One is valid for a/h=10, the second for a/h=25 and 50, and the last one for a/h=75. For thicker shells, the appearance of fourth-order theories follows a vertical direction from the center to the boundaries. For thinner shells, the direction is diagonal.

- As well-known, the error ranges vary significantly with thickness. The maximum values are 5% for a/h=75 and 10% for a/h=25. In other words, the use of FSDT is more reliable as a/h increases.

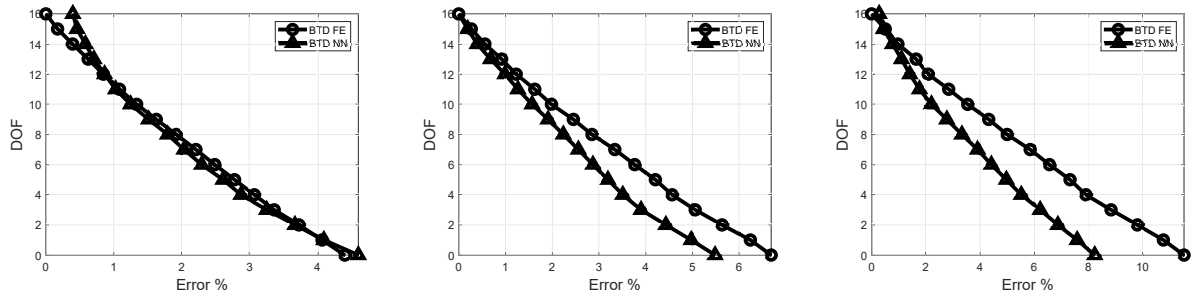


(a) a/h=75, training with a/h=50 and 100 (b) a/h=50, training with a/h=25 and 75 (c) a/h=25, training with a/h=10 and 50

Figure 12: BTD for 0/90/0 and various a/h

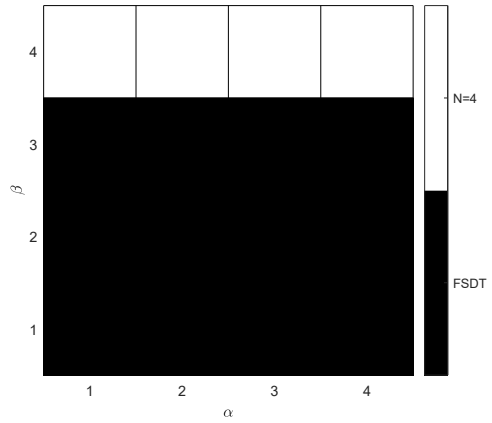


(a) FE, twelve FSDT, E=7.9 %

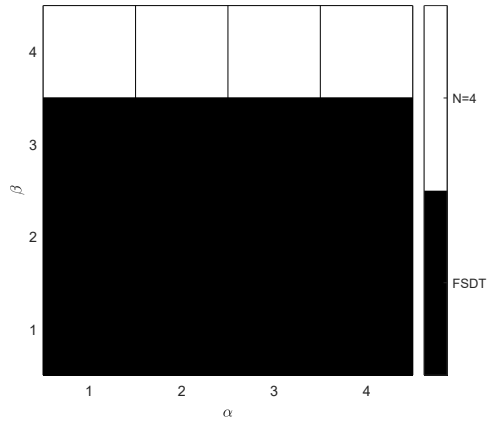


(b) NN, twelve FSDT, E=5.5 %

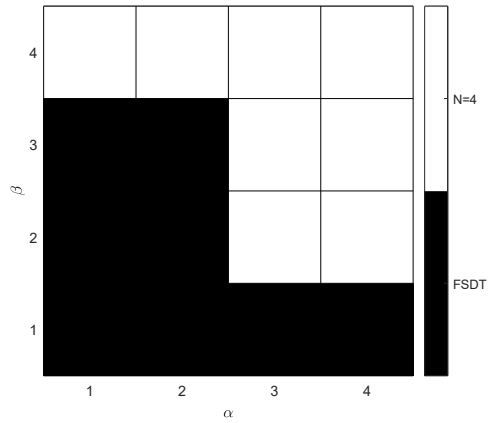


(c) FE, eight FSDT, E=5.0 %

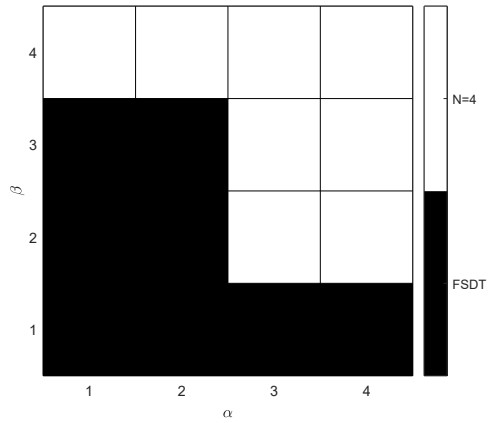


(d) NN, eight FSDT, E=3.3 %

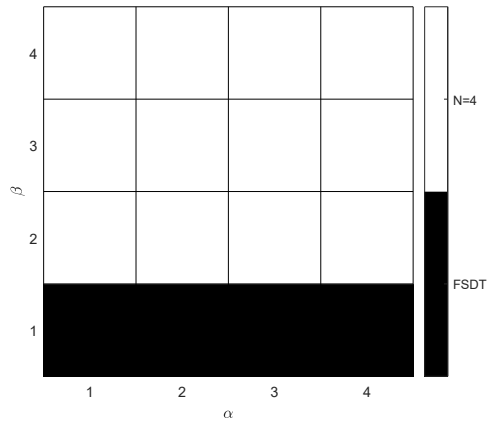


(e) FE, four FSDT, E=2.1 %

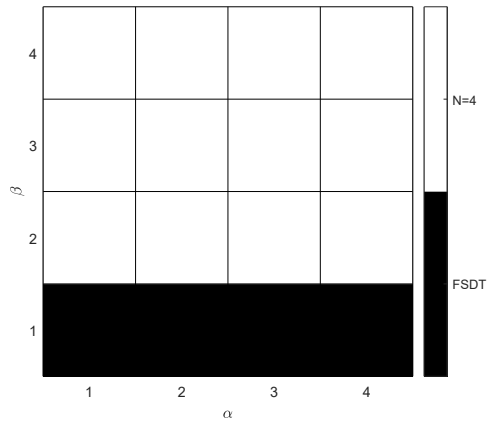


(f) NN, four FSDT, E=1.4 %

Figure 13: Best mesh distributions for 0/90/0, a/h=25, training with a/h=10 and 50

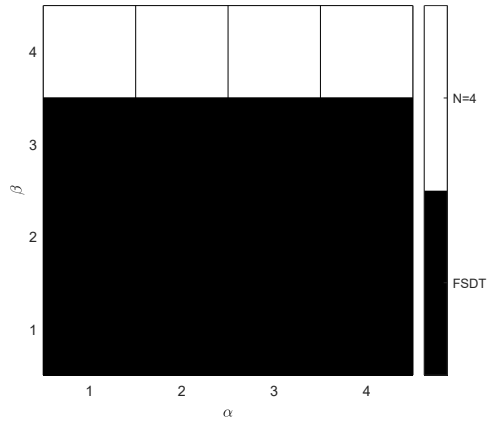


(a) FE, twelve FSDT, E=4.6 %

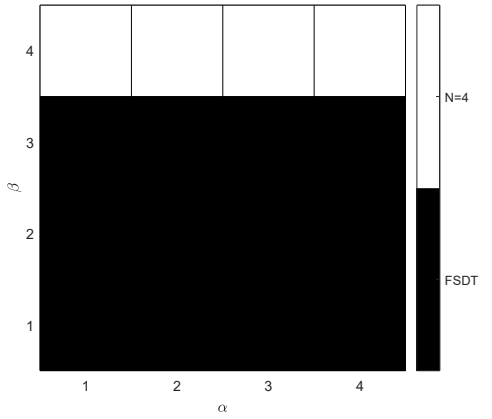


(b) NN, twelve FSDT, E=3.5 %

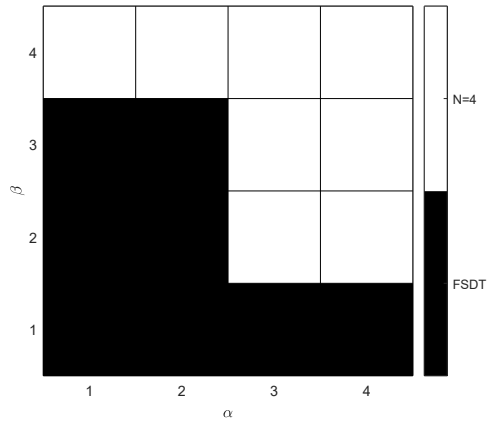


(c) FE, eight FSDT, E=2.9 %

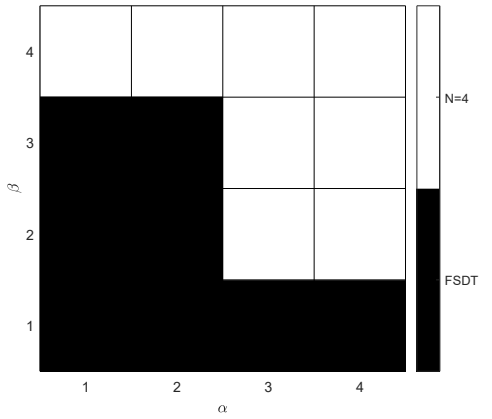


(d) NN, eight FSDT, E=2.2 %

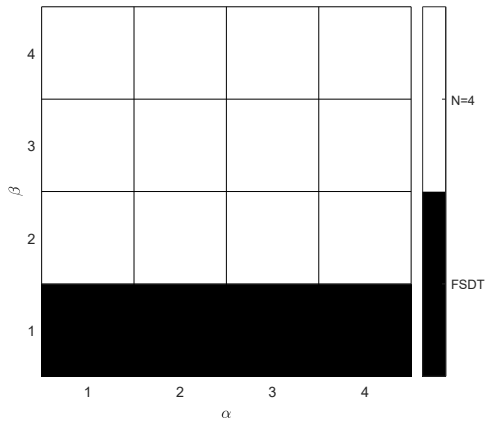


(e) FE, four FSDT, E=1.2 %

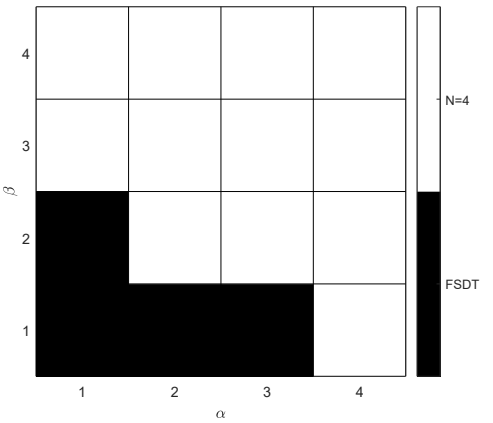


(f) NN, four FSDT, E=0.9 %

Figure 14: Best mesh distributions for 0/90/0, a/h=50, training with a/h=25 and 75)

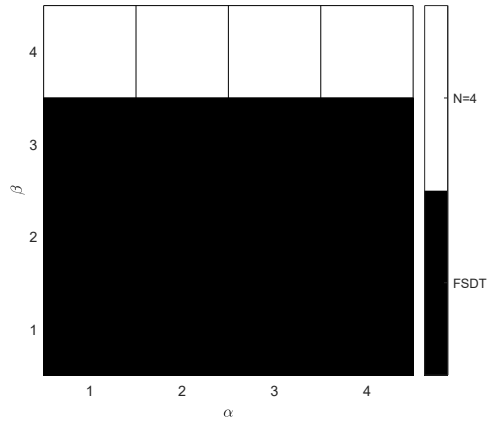


(a) FE, twelve FSDT, E=4.6 %

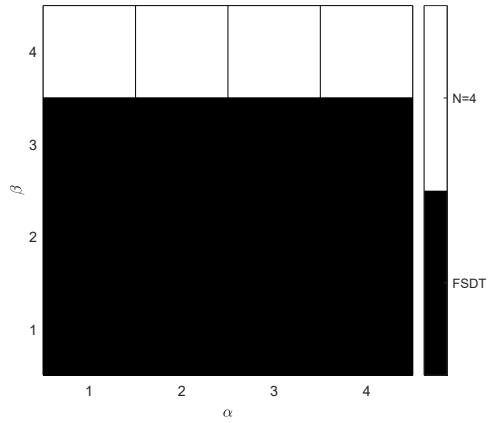


(b) NN, twelve FSDT, E=4.7 %

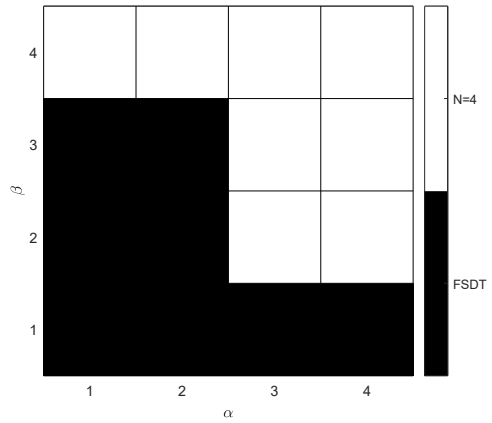


(c) FE, eight FSDT, E=1.9 %

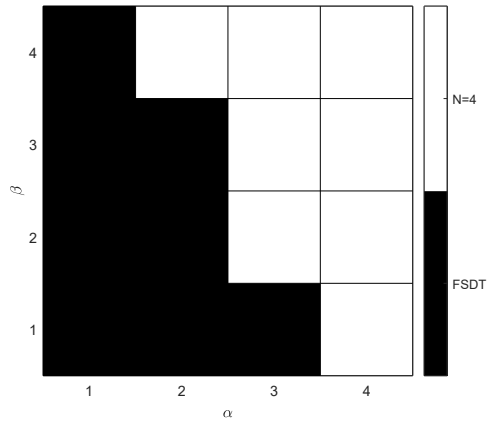


(d) NN, eight FSDT, E=1.8 %

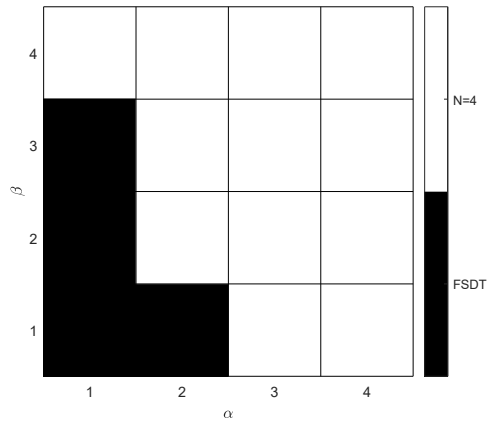


(e) FE, four FSDT, E=0.9 %

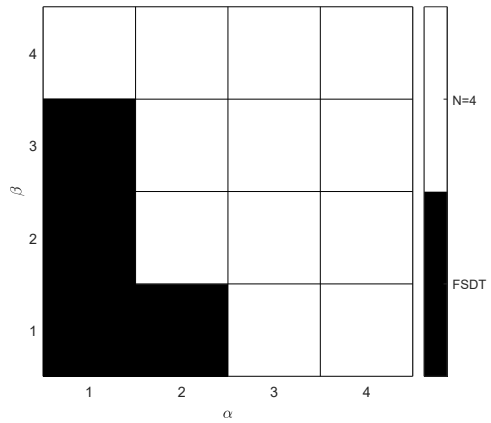


(f) NN, four FSDT, E=0.9 %

Figure 15: Best mesh distributions for 0/90/0, a/h=75, training with a/h=50 and 100)

# 6 Conclusions

This paper has proposed a novel use of neural networks (NN) as estimators of critical zones over shell finite element (FE) meshes concerning the presence of non-classical effects requiring higher-order kinematics. The approach makes use of the Carrera unified formulation (CUF) to generate any-order structural theory; the node-dependent kinematics (NDK) to assign different shell theories to FE nodes; NN is then trained using the FE results. The inputs of the training are the shell theories assigned to each element and the thickness of the structure. The target is the error over the first ten natural frequencies. The NN architecture has three to six layers and 10 to 20 neurons per layer. The size of the training set is one-tenth of the all possible combinations of mesh distributions required by FE to evaluate the best shell theory for every element. The numerical results considered various stacking sequences, boundary conditions, and thickness ratios. The analysis of the results shows that

- NN is accurate enough to substitute FE with a significant reduction of computational costs. N requires some 10% of the computational time of FE. The NN training can incorporate physical features of the problems such as the thickness ratio allowing to obtain results without the need for new FE analyses and preprocessing.

- The performances of NN can lead to the analysis of more complex structural configurations requiring larger FE models or iterations due to nonlinearities or optimization procedures.

- Concerning the most critical zones of the mesh, the presence of geometrical boundary conditions, as well-known, is the main feature to consider. However, changes in the type of constraints - supported or clamped -, stacking sequence and thickness can significantly affect the distribution of the critical areas. As a general guideline for thin shells, the areas demanding the use of refined models are in the proximity of the higher deformations. For thick shells, on the other hand, the vicinity of boundary conditions is a more significant indicator.

- The accuracy of the various mesh distributions can change significantly. For thick shells, in particular, errors higher than 10% may appear.

- Potential critical aspects of this approach emerged as the training considered simultaneously thin and thick shells. Such a scenario requires further investigations and the adoption of more advanced NN architectures as those developed in the scientific machine learning scenario.

The synergy between CUF and NN is promising given that the former can provide thousands of data sets in minutes and benchmarking for the rigorous assessment of results; the latter can increase the computational efficiency and widen the applicability of virtual modeling. Future investigations should focus on the use of NN for multiple targets, e.g., multi-point stress values, and the addition of more physical features in the training process, such as material properties and boundary conditions.

## References


[1] A. L. Cauchy. Sur l'équilibre et le mouvement d'une plaque solide. *Exercises de Matematique*, 3:328–355, 1828.

[2] S. D. Poisson. Memoire sur l'équilibre et le mouvement des corps elastique. *Mem. Acad. Sci.*, 1829.

[3] A.E.H. Love. *The Mathematical Theory of Elasticity.* Cambridge Univ Press, fourth edition, 1927.

[4] G. Kirchhoff. Uber das gleichgewicht und die bewegung einer elastischen scheibe. *Journal fur reins und angewandte Mathematik*, 40:51–88, 1850.

[5] E. Reissner. The effect of transverse shear deformation on the bending of elastic plates. *Journal of Applied Mechanics*, 12:69–76, 1945.

[6] R.D. Mindlin. Influence of rotatory inertia and shear in flexural motions of isotropic elastic plates. *Journal of Applied Mechanics*, 18:1031–1036, 1951.

[7] E. Carrera, A. Pagani, and S. Valvano. Shell elements with through-the-thickness variable kinematics for the analysis of laminated composite and sandwich structures. *Composites Part B: Engineering*, 111:294 – 314, 2017.

[8] G. Li, E. Carrera, M. Cinefra, A.G. de Miguel, A. Pagani, and E. Zappino. An adaptable refinement approach for shell finite element models based on node-dependent kinematics. *Composite Structures*, 210:1 – 19, 2019.

[9] S.A. Ambartsumian. Nontraditional theories of shells and plates. *Applied Mechanics Reviews*, 55(5):R35–R44, 2002.

[10] E. Carrera. Theories and finite elements for multilayered, anisotropic, composite plates and shells. *Archives of Computational Methods in Engineering*, 9(2):87–140, 2002.

[11] S.G. Lekhnitskii. Strength calculation of composite beams. *Vestnik inzhen i tekhnikov*, 9, 1935.

[12] F.B. Hildebrand, E. Reissner, and G.B. Thomas. Notes on the foundations of the theory of small displacements of orthotropic shells. *NACA TN-1833*, 1949.

[13] W.T. Koiter. A consistent first approximation in the general theory of thin elastic shells. *Proceedings of Symposium on the Theory of Thin Elastic Shells, August 1959, North-Holland, Amsterdam*, pages 12–23, 1959.

[14] S.A. Ambartsumian. Contributions to the theory of anisotropic layered shells. *Applied Mechanics Reviews*, 15:245–249, 1962.

[15] N.J. Pagano. Exact solutions for composite laminates in cylindrical bending. *Journal of Composite Materials*, 3(3):398–411, 1969.

[16] A.W. Leissa. Vibration of shells. *NASA-SP-288*, LC-77-186367, 1973.

[17] E.I. Grigolyuk and G.M. Kulikov. General directions of the development of theory of shells. *Mechanics of Composite Materials*, 24(287–298), 1988.

[18] K. Kapania. A review on the analysis of laminated shells. *ASME Journal of Pressure Vessel Technology*, 111(2):88–96, 1989.

[19] A.K. Noor and W.S. Burton. Assessment of computational models for multilayered composite shells. *Applied Mechanics Reviews*, 43(4):67–97, 1989.

[20] M. Touratier. A generalization of shear deformation theories for axisymmetric multilayered shells. *International Journal of Solids and Structures*, 29(11):1379 – 1399, 1992.

[21] V.V. Vasil'Ev and S.A. Lur'E. On refined theories of beams, plates, and shells. *Journal of Composite Materials*, 26(4):546–557, 1992.

[22] J. N. Reddy and D. H. Robbins. Theories and computational models for composite laminates. *Applied Mechanics Reviews*, 47(6):147–165, 1994.

[23] J.N. Reddy. Exact solutions of moderately thick laminated shells. *Journal of Engineering Mechanics*, 110(5):794–809, 1984.

[24] J.N. Reddy and C.F. Liu. A higher-order shear deformation theory of laminated elastic shells. *International Journal of Engineering Science*, 23(3):319 – 330, 1985.

[25] M. Qatu. Recent research advances in the dynamic behavior of shells: 1989-2000, part 1: Laminated composite shells. *Applied Mechanics Review*, 55(4):325–350, 2002.

[26] M. Qatu, R.W. Sullivan, and W. Wang. Recent research advances on the dynamic analysis of composite shells: 2000–2009. *Composite Structures*, 93(1):14 – 31, 2010.

[27] H.V. Lakshminarayana and K. Dwarakanath. Free vibration characteristics of cylindrical shells made of composite materials. *Journal of Sound and Vibration*, 154(3):431 – 439, 1992.

[28] J. Zhu. Free vibration analysis of multilayered composite plates and shells with the natural approach. *Computer Methods in Applied Mechanics and Engineering*, 130(1):133 – 149, 1996.

[29] N.S. Bardell, J.M. Dunsdon, and R.S. Langley. Free and forced vibration analysis of thin, laminated, cylindrically curved panels. *Composite Structures*, 38(1):453 – 462, 1997.

[30] T. Park, K. Kim, and S. Han. Linear static and dynamic analysis of laminated composite plates and shells using a 4-node quasi-conforming shell element. *Composites Part B: Engineering*, 37(2):237 – 248, 2005.

[31] H. Nguyen-Van, N. Mai-Duy, and T. Tran-Cong. Free vibration analysis of laminated plate/shell structures based on fsdt with a stabilized nodal-integrated quadrilateral element. *Journal of Sound and Vibration*, 313(1):205 – 223, 2008.

[32] H. Nguyen-Van, N. Mai-Duy, W. Karunasena, and T. Tran-Cong. Buckling and vibration analysis of laminated composite plate/shell structures via a smoothed quadrilateral flat shell element with in-plane rotations. *Computers and Structures*, 89(7):612 – 625, 2011.

[33] D. Chakravorty, J.N. Bandyopadhyay, and P.K. Sinha. Finite element free vibration analysis of point supported laminated composite cylindrical shells. *Journal of Sound and Vibration*, 181(1):43 – 52, 1995.

[34] K.S.S. Ram and T.S. Babu. Free vibration of composite spherical shell cap with and without a cutout. *Computers and Structures*, 80(23):1749 – 1756, 2002.

[35] S.C. Han, S. Choi, and S.Y. Chang. Nine-node resultant-stress shell element for free vibration and large deflection of composite laminates. *Journal of Aerospace Engineering*, 19(2):103–120, 2006.

[36] S. Jayasankar, S. Mahesh, S. Narayanan, and C. Padmanabhan. Dynamic analysis of layered composite shells using nine node degenerate shell elements. *Journal of Sound and Vibration*, 299(1):1 – 11, 2007.

[37] R.K. Khare, T. Kant, and A.K. Garg. Free vibration of composite and sandwich laminates with a higher-order facet shell element. *Composite Structures*, 65(3):405 – 418, 2004.

[38] R.K. Khare, A.K. Garg, and T. Kant. Free vibration of sandwich laminates with two higher-order shear deformable facet shell element models. *Journal of Sandwich Structures & Materials*, 7(3):221–244, 2005.

[39] A. Kumar, P. Bhargava, and A. Chakrabarti. Vibration of laminated composite skew hypar shells using higher order theory. *Thin-Walled Structures*, 63:82 – 90, 2013.

[40] S.N. Thakur and C. Ray. An accurate C0 finite element model of moderately thick and deep laminated doubly curved shell considering cross sectional warping. *Thin-Walled Structures*, 94:384 – 393, 2015.

[41] W.H. Lee and S.C. Han. Free and forced vibration analysis of laminated composite plates and shells using a 9-node assumed strain shell element. *Computational Mechanics*, 39(1):41–58, 2006.

[42] D. Chronopoulos, M. Ichchou, B. Troclet, and O. Bareille. Efficient prediction of the response of layered shells by a dynamic stiffness approach. *Composite Structures*, 97:401 – 404, 2013.

[43] D. He, D. Shi, Q. Wang, and C. Shuai. Wave based method (wbm) for free vibration analysis of cross-ply composite laminated cylindrical shells with arbitrary boundaries. *Composite Structures*, 213:284 – 298, 2019.

[44] X. Xie, G. Jin, Y. Yan, S.X. Shi, and Z. Liu. Free vibration analysis of composite laminated cylindrical shells using the haar wavelet method. *Composite Structures*, 109:169 – 177, 2014.

[45] X. Xie, G. Jin, W. Li, and Z. Liu. A numerical solution for vibration analysis of composite laminated conical, cylindrical shell and annular plate structures. *Composite Structures*, 111:20 – 30, 2014.

[46] O. Civalek. Numerical analysis of free vibrations of laminated composite conical and cylindrical shells: Discrete singular convolution (dsc) approach. *Journal of Computational and Applied Mathematics*, 205(1):251 – 271, 2007.

[47] O. Civalek. Vibration analysis of laminated composite conical shells by the method of discrete singular convolution based on the shear deformation theory. *Composites Part B: Engineering*, 45(1):1001 – 1009, 2013.

[48] K.K. Viswanathan, S. Javed, K. Prabakar, Z.A. Aziz, and I.A. Bakar. Free vibration of anti-symmetric angle-ply laminated conical shells. *Composite Structures*, 122:488 – 495, 2015.

[49] Q. Wang, D. Shao, and B. Qin. A simple first-order shear deformation shell theory for vibration analysis of composite laminated open cylindrical shells with general boundary conditions. *Composite Structures*, 184:211 – 232, 2018.

[50] B. Cheng and D.M. Titterington. Neural networks: A review from a statistical perspective. *Statistical Science*, 9(1):2–30, 02 1994.

[51] H. El Kadi. Modeling the mechanical behavior of fiber-reinforced polymeric composite materials using artificial neural networks—a review. *Composite Structures*, 73(1):1 – 23, 2006.

[52] K. Worden, W.J. Staszewski, and J.J. Hensman. Natural computing for mechanical systems research: A tutorial overview. *Mechanical Systems and Signal Processing*, 25(1):4 – 111, 2011.

[53] S. Nasiri, M.R. Khosravani, and K. Weinberg. Fracture mechanics and mechanical fault detection by artificial intelligence methods: A review. *Engineering Failure Analysis*, 81:270 – 293, 2017.

[54] G. Balokas, S. Czichon, and R. Rolfes. Neural network assisted multiscale analysis for the elastic properties prediction of 3D braided composites under uncertainty. *Composite Structures*, 183:550 – 562, 2018. In honor of Prof. Y. Narita.

[55] L. Cappelli, G. Balokas, M. Montemurro, F. Dau, and L. Guillaumat. Multi-scale identification

of the elastic properties variability for composite materials through a hybrid optimisation strategy. *Composites Part B: Engineering*, 176:107193, 2019.

[56] U.K. Mallela and A. Upadhyay. Buckling load prediction of laminated composite stiffened panels subjected to in-plane shear using artificial neural networks. *Thin-Walled Structures*, 102:158 – 164, 2016.

[57] C. Suresh Kumar, V. Arumugam, R. Sengottuvelusamy, S. Srinivasan, and H. N. Dhakal. Failure strength prediction of glass/epoxy composite laminates from acoustic emission parameters using artificial neural network. *Applied Acoustics*, 115:32 – 41, 2017.

[58] M.G. Vineela, A. Dave, and P.K. Chaganti. Artificial neural network based prediction of tensile strength of hybrid composites. *Materials Today: Proceedings*, 5(9, Part 3):19908 – 19915, 2018. Materials Processing and characterization, 16th – 18th March 2018.

[59] X. Liu, F. Gasco, J. Goodsell, and W. Yu. Initial failure strength prediction of woven composites using a new yarn failure criterion constructed by deep learning. *Composite Structures*, 230:111505, 2019.

[60] G. Chen, H. Wang, A. Bezold, C. Broeckmann, D. Weichert, and L. Zhang. Strengths prediction of particulate reinforced metal matrix composites (PRMMCs) using direct method and artificial neural network. *Composite Structures*, 223:110951, 2019.

[61] R.A. Cidade, D.S.V. Castro, E.M. Castrodeza, P. Kuhn, G. Catalanotti, J. Xavier, and P.P. Camanho. Determination of mode I dynamic fracture toughness of IM7-8552 composites by digital image correlation and machine learning. *Composite Structures*, 210:707 – 714, 2019.

[62] S. Dey, S. Naskar, T. Mukhopadhyay, U. Gohs, A. Spickenheuer, L. Bittrich, S. Sriramula, S. Adhikari, and G. Heinrich. Uncertain natural frequency analysis of composite plates including effect of noise – a polynomial neural network approach. *Composite Structures*, 143:130 – 142, 2016.

[63] S. Dey, T. Mukhopadhyay, A. Spickenheuer, U. Gohs, and S. Adhikari. Uncertainty quantification in natural frequency of composite plates - an artificial neural network based approach. *Advanced Composites Letters*, 25(2):096369351602500203, 2016.

[64] P.K. Karsh, T. Mukhopadhyay, and S. Dey. Stochastic dynamic analysis of twisted functionally graded plates. *Composites Part B: Engineering*, 147:259 – 278, 2018.

[65] M. Stoffel, R. Gulakala, F. Bamer, and B. Markert. Artificial neural networks in structural dynamics: A new modular radial basis function approach vs. convolutional and feedforward topologies. *Computer Methods in Applied Mechanics and Engineering*, 364:112989, 2020.

[66] C. Zimmerling, D. Dörr, F. Henning, and L. Kärger. A machine learning assisted approach for textile formability assessment and design improvement of composite components. *Composites Part A: Applied Science and Manufacturing*, 124:105459, 2019.

[67] N. Zobeiry, D. van Ee, A. Floyd, and A. Poursartip. Theory-guided machine learning composites processing modelling for manufacturability assessment in preliminary design. In NAFEMS, editor, *Proceedings of the 2019 NAFEMS World Congress*.

[68] H. Yao, Y. Gao, and Y. Liu. Fea-net: A physics-guided data-driven model for efficient mechanical response prediction. *Computer Methods in Applied Mechanics and Engineering*, 363:112892, 2020.

[69] L. Liang, L. Minliang, M. Caitlin, and S. Wei. A deep learning approach to estimate stress distribution: a fast and accurate surrogate of finite-element analysis. *Journal of The Royal Society Interface*, 15(138):20170844, 2018.

[70] G. Capuano and J.J. Rimoli. Smart finite elements: A novel machine learning application. *Computer Methods in Applied Mechanics and Engineering*, 345:363 – 381, 2019.

[71] J. Gajewski, P. Golewski, and T. Sadowski. Geometry optimization of a thin-walled element for an air structure using hybrid system integrating artificial neural network and finite element method. *Composite Structures*, 159:589 – 599, 2017.

[72] A. Albanesi, N. Roman, F. Bre, and V. Fachinotti. A metamodel-based optimization approach to reduce the weight of composite laminated wind turbine blades. *Composite Structures*, 194:345 – 356, 2018.

[73] E. Carrera. Theories and finite elements for multilayered plates and shells: a unified compact formulation with numerical assessment and benchmarking. *Archives of Computational Methods in Engineering*, 10(3):216–296, 2003.

[74] E. Carrera, M. Cinefra, M. Petrolo, and E. Zappino. *Finite Element Analysis of Structures through Unified Formulation*. John Wiley & Sons, Chichester, 2014.

[75] E. Carrera and M. Petrolo. Guidelines and recommendation to construct theories for metallic and composite plates. *AIAA Journal*, 48(12):2852–2866, 2010.

[76] E. Carrera and M. Petrolo. On the effectiveness of higher-order terms in refined beam theories. *Journal of Applied Mechanics*, 78, 2011.

[77] E. Carrera, M. Cinefra, A. Lamberti, and M. Petrolo. Results on best theories for metallic and laminated shells including layer-wise models. *Composite Structures*, 126:285–298, 2015.

[78] M. Petrolo and E. Carrera. Best theory diagrams for multilayered structures via shell finite elements. *Advanced Modeling and Simulation in Engineering Science*, 6(4):1–23, 2019.

[79] K.J. Bathe and E.N. Dvorkin. A formulation of general shell elements—the use of mixed interpolation of tensorial components. *International Journal for Numerical Methods in Engineering*, 22(3):697–722, 1986.

[80] M. T. Hagan, H. B. Demuth, M. H. Beale, and O. De Jesús. *Neural Network Design*. Martin Hagan, 2014.

[81] M. Cinefra. Free-vibration analysis of laminated shells via refined MITC9 elements. *Mechanics of Advanced Materials and Structures*, 23(9):937–947, 2016.

[82] M. Petrolo and E. Carrera. Methods and guidelines for the choice of shell theories. *Acta Mechanica*, 231:395–434, 2020.

[83] M. Petrolo and E. Carrera. Best spatial distributions of shell kinematics over 2d meshes for free vibration analyses. Submitted.

[84] E. Carrera. The effects of shear deformation and curvature on buckling and vibrations of cross-ply laminated composite shells. *Journal of Sound and Vibrations*, 150(3):405–433, 1991.